Renato S.M. Almeida ; Si'an Chen ; Benjamin Besser ; Kamen Tushtev ; Yang Li ; Kurosch Rezwan

Fatigue behavior and damage analysis of PIP C/SiC composite

Journal Article as: peer-reviewed accepted version (Postprint)

DOI of this document*(secondary publication): https://doi.org/10.26092/elib/3445

Publication date of this document: 08/11/2024

* for better findability or for reliable citation

Recommended Citation (primary publication/Version of Record) incl. DOI:

Renato S.M. Almeida, Si'an Chen, Benjamin Besser, Kamen Tushtev, Yang Li, Kurosch Rezwan,
Fatigue behavior and damage analysis of PIP C/SiC composite,
Journal of the European Ceramic Society, Volume 42, Issue 13, 2022, Pages 5391-5398, ISSN 0955-2219,
https://doi.org/10.1016/j.jeurceramsoc.2022.06.053.

Fatigue behavior and damage analysis of PIP C/SiC composite

Renato S.M. Almeida [b], Si'an Chen [a,*], Benjamin Besser [c], Kamen Tushtev [b], Yang Li [d,e,**], Kurosch Rezwan [b,f]

[a] Science and Technology on Advanced Ceramic Fibers and Composites Laboratory, National University of Defense Technology, Changsha 410083, China
[b] Advanced Ceramics, University of Bremen, Bremen 28359, Germany
[c] Center for Environmental Research and Sustainable Technology (UFT), University of Bremen, Bremen 28359, Germany
[d] National Key Laboratory of Science and Technology on High-strength Structural Materials, Central South University, Changsha 410083, China
[e] Powder Metallurgy Research Institute, Central South University, Changsha 410083, China
[f] MAPEX - Center for Materials and Processes, University of Bremen, Bremen 28359, Germany

ARTICLE INFO

Keywords:
Ceramic matrix composites
Fatigue
Damage analysis
Acoustic emission
Residual strength

ABSTRACT

In this work, we study the fatigue behavior of a C/SiC composite produced by several cycles of polymer infiltration and pyrolysis (PIP). Fatigue tests were performed with maximum stresses corresponding to 60–90% of the tensile strength of the composite. During the fatigue tests, acoustic emission (AE) monitoring was performed and the measured AE energy was utilized to quantify the damage and distinguish possible damage mechanisms. Most of the fatigue damage in the form of matrix cracking, interface damage and fiber breakage occurs in the first cycle. As loading cycles proceeded, damage in form of matrix crack re-opening and interfacial friction constantly accumulates. Nevertheless, all samples survived the run-out of 1,000,000 cycles. After the fatigue tests, an increase of the tensile strength is observed. This phenomenon is associated with the relief of process-induced internal thermal stresses and the weakening of the fiber-matrix interface. In general, the studied material shows very high relative fatigue limit of 90% of its tensile strength.

1. Introduction

Ceramic matrix composites (CMCs) combine the inherent hardness and thermal/chemical stability of ceramics with a higher damage tolerance due to fiber reinforcement. Among this class of materials, carbon fiber reinforced silicon carbide (C/SiC) composites distinguish themselves due to their low density, high specific strength and modulus, as well as excellent thermal shock resistance [1–3]. Hence, C/SiC composites are of interest for the production of high-temperature structural components for aerospace, advanced friction systems and energy industry applications. For instance, current C/SiC composites are used for panels, winglets, lifting wings and fuselage doors in recoverable spacecraft, thermal protection systems of space shuttles, space mirrors, etc [4].

During the aforementioned applications, high-frequency vibrations caused by noise in operation conditions, as well as mechanical and thermal stresses caused by high-speed air scouring, can lead to the failure of components due to fatigue [3,5,6]. Therefore, fatigue resistance is one of the key factors that determines the structural reliability and stability for such applications, in particular, if human lives depend on it. Hence, the study of the fatigue behavior and post-fatigue properties is of great importance for the development of not only C/SiC composites, but CMCs in general. In this sense, many works about tensile fatigue tests of C/SiC and SiC/SiC at room or elevated temperatures can be found in the literature [7–11]. CMCs generally show high fatigue limits, which depends on the induced fatigue damage that is rather complex [12–16]. The fatigue damage can also influence the post-fatigue mechanical behavior of the composites. It has been reported that the interfacial variation and crack multiplication under tensile fatigue stress can either increase or decrease the residual strength of CMCs [10,13,17]. Therefore, some researchers focus on studying the damage development during fatigue loading of CMCs. For instance, Morscher et al. [18,19] investigated the fracture behavior of SiC/SiC composites during loading-unloading processes via acoustic emission monitoring (AE). In our previous work [20], AE was also used to describe the fatigue damage type, which was then related to the stress-strain response of

* Corresponding author.
** Corresponding author at: National Key Laboratory of Science and Technology on High-strength Structural Materials, Central South University, Changsha 410083, China.
E-mail addresses: chensian07@nudt.edu.cn (S. Chen), liyang16@csu.edu.cn (Y. Li).

2.5D C/C-SiC composites after fatigue loading. Furthermore, Momon et al. [21] studied the fatigue life prediction of different SiC-based CMCs during static fatigue tests with periodical unloading/reloading sequences by combining the coefficient of emission obtained by AE detection.

In summary, the fatigue behavior and post-fatigue properties of CMCs depend on their complicated damage characteristics, which can be influenced by fiber architecture, interface, preparation process and matrix of the composites. These interactions and their impact on material properties are not fully understood yet and need further investigation. Therefore, more experimental data related to the mechanical behavior and damage development under static and dynamic stresses will facilitate the understanding of fatigue and enable improved design for reliability of CMCs. Hence, the objective of this work is to investigate the mechanical response of a high-strength 2D C/SiC composite, prepared by polymer infiltration and pyrolysis (PIP), to applied cyclic mechanical loads. In general, PIP C/SiC composites show high application potential for the production of big-size components due to low processing temperatures and near-net-shape technology [22]. Nevertheless, there is a lack of fatigue studies on PIP C/SiC composites in the literature. In this work, fatigue tests with different stress levels were performed. The loading-unloading process was monitored by AE and by measuring the dynamic modulus. Afterwards, samples that survived the fatigue loading were characterized with quasi-static tensile tests. Fatigue damage is analyzed based on AE analysis as well as the post-fatigue behavior and the fracture surface of the tested specimens.

2. Experimental procedure

2.1. C/SiC composite

The studied material is a PIP C/SiC composite with 2D fiber reinforcement. Plain carbon cloths of 1 K PAN based carbon fibers (Toray T300B) were used as reinforcement. A total of twenty 200 × 200 mm^2 carbon fiber cloths were cut, stacked and stitched together with two stitches per centimeter. The fiber pre-form was then infiltrated under vacuum by a polycarbosilane/xylene solution with a mass ratio of 1:1 and cured at 150 °C for 6 h. The polycarbosilane was synthesized in the lab with a molecular weight of ~1300 and softening point of ~210 °C. Afterwards, the infiltrated fiber pre-form was pyrolyzed under inert gas at 1200 °C for 2 h with heating rate of 15 °C/min. The infiltration-pyrolysis procedure was repeated seven times. The repeated pyrolysis cycles at relatively low temperatures were performed in order to reduce possible process-induced defects on the material. A more detailed description of the processing method can be found in Ref. [22]. An example micrograph of the C/SiC composite microstructure can be seen in Fig. 1a, while its main properties are given in Table 1.

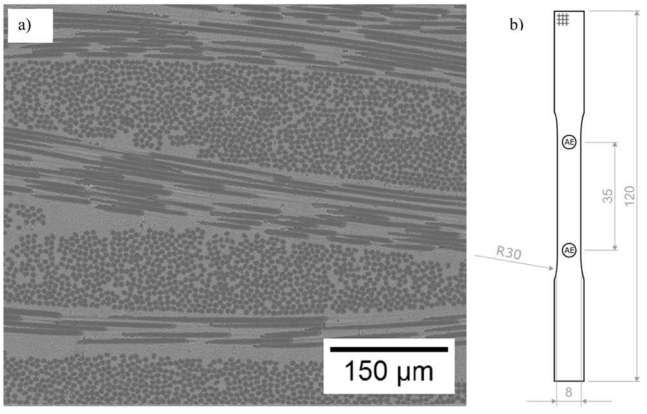

Fig. 1. (a) Typical microstructure of C/SiC composite. (b) Dog-bone specimen geometry for mechanical tests with AE sensors.

Table 1
Measured physical properties of PIP C/SiC composite. Values of tensile strength and elastic modulus were calculated from quasi-static tensile tests on three samples.

Sample	Fiber content (%)	Bulk density (g/cm^3)	Open porosity (%)	Tensile strength (MPa)	Elastic modulus (GPa)
C/SiC	45–50	1.93	3–5	217 ± 13	94.7 ± 2.4

2.2. Mechanical characterization

For the mechanical tests, dog-bone samples with a reduced cross-section of 3 × 8 mm^2 were prepared by wire eroding (see Fig. 1b). All samples were ground and polished to obtain flat surfaces. The mechanical tests were performed using a servo-hydraulic testing machine Roell-Amsler System Rel 2100 (Zwick Roell Group, Ulm, Germany) with a MTS Flex Test 40 controller. The machine is equipped with 25 kN load cell to measure the applied force and a linear variable differential transformer position sensor to measure the displacement. Furthermore, the deformation of the samples was measured directly using an axial extensometer 632.27F-30 (MTS Systems, Eden Prairie, MN, USA). Data acquisition was performed with measuring rate of 260 Hz. During the mechanical tests, AE monitoring was performed using an AMSY 4 system (Vallen Systeme GmbH, Icking, Germany) with two AE sensors VS 600-Z2 (400–800 kHz and Ø 4.7 mm). The sensors were glued to the samples with a distance of approximately 35 mm between each other using hot glue (see Fig. 1b). For AE hit detection, a threshold of 48.3 dB, duration discrimination time of 100 µs and rearm time of 1000 µs were used. Before the tests, the velocity of AE propagation in the specimen was measured. This was used for linear location of AE events during the mechanical tests by measuring the difference of measuring time between the two AE sensors. Only signals measured between the two sensors were considered for data analysis.

Tensile-tensile fatigue tests were performed in accordance to the standard ASTM C1360. The maximum fatigue stress was determined in accordance to the previously measured tensile strength of as-processed specimens (see Table 1). The selected maximum fatigue stress levels were of 60–90% of the tensile strength of the composite. Three samples were tested per stress level. During the tests, the samples were first loaded to the mean stress and then fatigue loaded under load control following a sinusoidal wave with frequency of 10 Hz and fatigue stress ratio of 0.1. To avoid early failure of the samples due to the high fatigue frequency, the maximum fatigue stress was slowly increased during the first cycles until achieving the selected stress level. Samples were tested until failure or until the run-out of 1,000,000 cycles was achieved. Stress-strain loops were periodically recorded until the end of the test. The dynamic moduli of the recorded cycles were calculated by performing a linear regression between the first and last stress/strain data point of the respective cycles. On the other hand, AE monitoring was performed constantly for the first 100,000 cycles. The number of AE events (hits) and their associated energy (1 eu = 10^{-18} J) were evaluated.

Samples that survived the fatigue loading were subsequently characterized with quasi-static tensile tests following the standard DIN EN 658-1. These samples were compared with as-processed specimens. The tensile tests were carried out with a constant loading speed of 1 mm/min until failure. AE monitoring was performed during the whole test. Afterwards, micrographs of the resulting fracture surfaces were taken using a scanning electron microscope Zeiss EVO 10 (ZEISS, Oberkochen, Germany) with an acceleration voltage of 15 kV.

3. Results

3.1. Fatigue tests

Fatigue tests were performed with stress levels of 60–90% of the as-processed tensile strength of the studied C/SiC composites. A summary of the fatigue test results can be seen in Table 2. All samples survived the run-out cycles, even with the maximum fatigue stress of 195 MPa (stress level of 90%), indicating a high fatigue strength of the studied composite.

An example of a stress-strain curve measured during fatigue loading with stress level of 70% is seen in Fig. 2a. Since not all loading–unloading cycles were recorded during the test, there are blank spaces in the curve. The load was slowly increased within the first cycles in order to avoid the early failure of the samples due to the high testing frequency of 10 Hz. Therefore, it is important to bear in mind that it takes approximately 50 cycles to reach the maximum/minimum set fatigue stress in order to understand the results presented below. Fig. 2b shows a few selected loading–unloading hysteresis loops from the curve shown in Fig. 2a. The area of the hysteresis loops can be used to calculate the amount of mechanical energy dissipated in the respective cycles. Comparing cycle 10 (1.5 kJ/m^2) with cycle 20 (5.8 kJ/m^2), it can be seen that, at first, the area of the loops increases. After 20 cycles, the area of the loops starts to decrease, reaching 4.2 kJ/m^2 on cycle 50, at which the fatigue stress reaches the set maximum fatigue stress. As the loading progresses, the area of the loops continues to decrease. For instance, cycle 1000 has an equivalent mechanical energy to 3.9 kJ/m^2, while cycle 900,000 has an equivalent mechanical energy of 3.3 kJ/m^2. Furthermore, it can be seen that the hysteresis loops start to get closer together.

For the damage analysis during the fatigue tests, AE monitoring was performed for the first 100,000 cycles. In addition, the dynamic modulus was calculated for the recorded cycles until the run-out of 1,000,000 cycles. The evolution of dynamic elastic modulus, cumulative AE hit count and total AE energy with the number of fatigue cycles is shown in Fig. 3 for each stress level. The overall behavior is very similar among the different stress levels, although bigger changes are seen for higher stress levels. In general, there is a rapid decrease of the elastic modulus during the first cycles before reaching the maximum stress. It should be noted that the relatively low dynamic moduli measured within cycles 2–5 are due to the fact that the cyclic loading is still not stable and the ratio between minimum and maximum stress is very high for these cycles (see Fig. 2a). After reaching the maximum stress, the decrease of dynamic modulus slows down as the loading progresses. However, even after 900,000 cycles, the dynamic modulus is still decreasing. This is more pronounced for samples tested with higher stress levels.

Most of the AE signals occur in the first cycle and the number of new events decreases as the loading progresses. Nevertheless, there is a different trend between AE hit count and AE energy. In general, the increase of AE energy follows a similar trend as decrease of dynamic modulus, showing considerable increases during the loading cycles until the maximum stress. The main difference between the two tendencies lies on the fact that the energy of the measured signals is very distinct during the several stages of the fatigue test. Taking the specimen tested with the fatigue stress level of 90% as an example (Fig. 3d), there is a wide range of AE signals measured during the first loading cycle. The energy of the signals is in the range of 3–560 eu, resulting in an average AE hit energy of about 25 eu on the first cycle. During the next cycles until the maximum fatigue stress, the average AE hit energy per cycle can reach up to 300 eu. Afterwards, the average AE energy starts to decrease and stays constant at about 10 eu after 1000 cycles.

Table 2
Summary of fatigue test results. All samples achieved the run-out of 1,000,000 cycles.

Stress level (%)	Maximum fatigue stress (MPa)	Frequency (Hz)	Cycles to failure
60	130	10	1,000,000
70	152	10	1,000,000
80	174	10	1,000,000
90	195	10	1,000,000

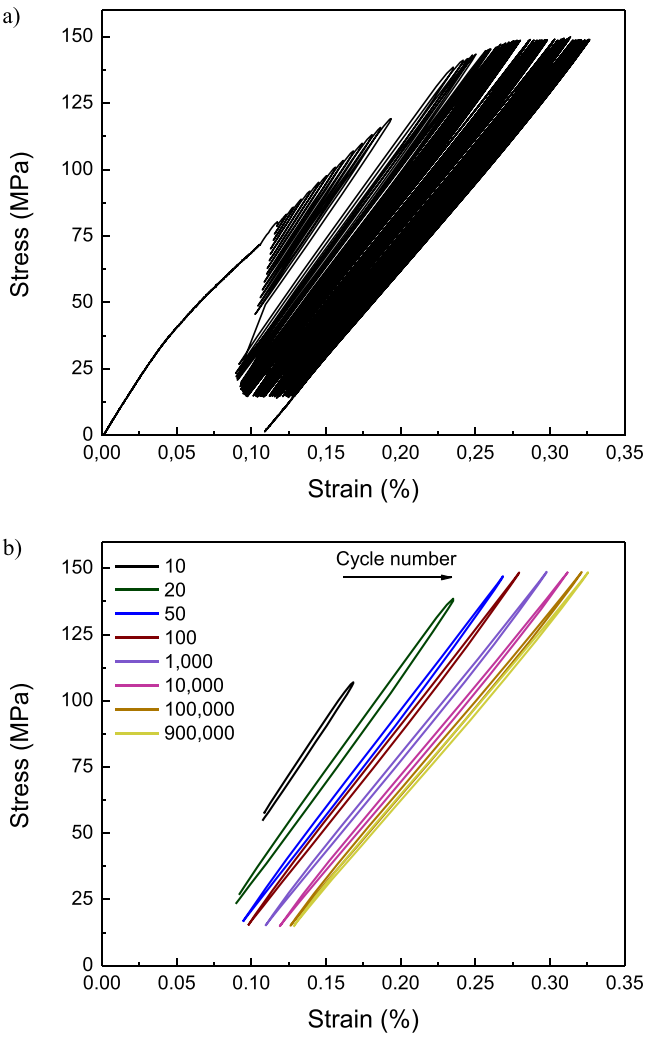

Fig. 2. Example of fatigue test with 1,000,000 cycles and stress level of 70%: (a) Stress strain curve during fatigue test and (b) stress-strain hysteresis loops of selected cycles.

When comparing the different stress levels, it can be seen that there is a higher decrease of dynamic modulus with higher stress levels. For instance, while the dynamic modulus decreases to 73 GPa when the material is subjected to a stress level of 60%, it reduces to about 62 GPa at the end of the fatigue test with stress level of 90%. Furthermore, while the modulus is more stable after 100,000 cycles with the stress level of 60%, there is a noticeable decreasing trend at the end of the fatigue loading with 90%. Differences can be seen in the AE data as well, especially considering the relative amount of AE hit count and AE energy that takes place in the first cycle. For instance, 55% of the total AE hit count take place in the first cycle for the fatigue test with 60%, while 69% occur in the first cycle for 90%. Hence, with higher maximum load in the first cycle, relatively more AE hits take place in the first cycle.

3.2. Quasi-static tensile tests

Tensile tests were carried out on samples before and after the fatigue loadings. Examples of stress-strain curves along with the measured

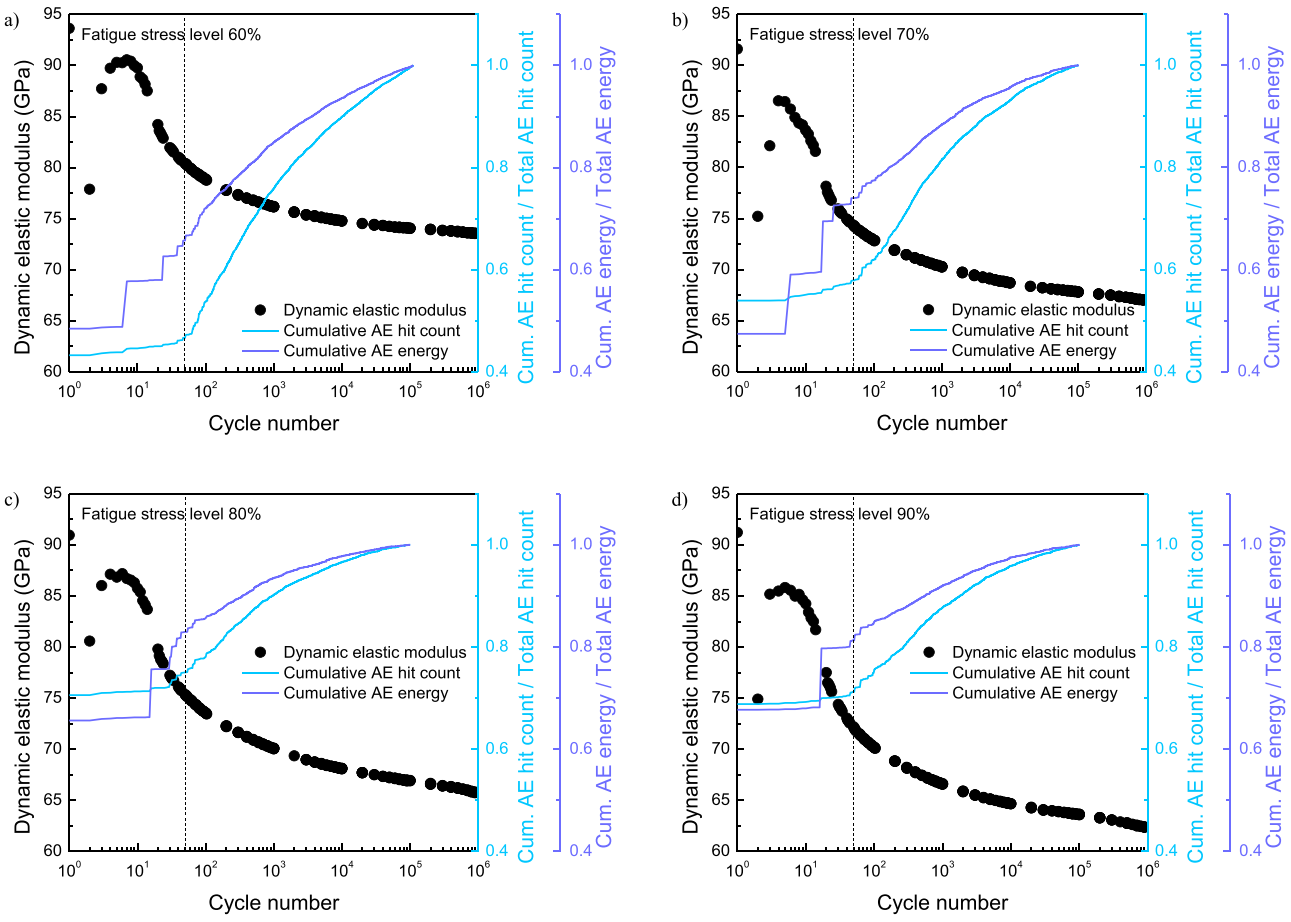

Fig. 3. Damage evolution in representative samples under fatigue loading with stress level of (a) 60%, (b) 70%, (c) 80% and (d) 90%. Dashed line shows when the set maximum fatigue stress was reached.

cumulative AE hit energy are shown in Fig. 4. In the as-processed state (Fig. 4a), the composite shows considerable non-linearity. The proportional limit, defined as the point in which the stress-strain curve deviates from the initial linear-elastic trend, was measured as 35 ± 1 MPa. It is important to note that the increase of AE activity occurs below the proportional limit at around 23 MPa. As the loading progresses, AE hits with higher energy are measured. Furthermore, cascaded hits with much higher energy were detected at the moment of failure (maximum stress). After the fatigue loadings, the mechanical behavior drastically changes. As seen in Fig. 4b-e, the fatigue-loaded composites show much a more extent linear region. In general, the material shows only linear-elastic deformation until reaching the previous maximum fatigue stress. The measured AE energy is also in accordance, showing a visible increase only at higher stresses.

The measured tensile strength and elastic modulus before and after the fatigue loadings are displayed in Fig. 5. There is an overall increase of tensile strength with fatigue stress level, which is more pronounced with the fatigue stress levels of 80% and 90%. On the other hand, the elastic modulus decreases after the fatigue loading, reaching a plateau at the stress level of 80%. This contrasts with the measured dynamic modulus measured during the fatigue loadings (see Fig. 3). Although the composite reaches lower dynamic modulus during the fatigue test of 90% in comparison to 80%, there is no statistical differences between the elastic moduli measured during the quasi-static tests after the fatigue loadings.

Further differences in mechanical behavior after the fatigue loadings can be seen when analyzing the fracture surface of the samples after the quasi-static tensile tests. Fig. 6 shows examples of fracture surfaces of samples previously fatigue loaded with stress levels of 70% and 90%. In general, samples previously fatigued with 60% and 70% show a very similar fracture morphology. The fracture takes place in different planes due to the different crack paths along matrix, 90° fiber layers and 0° fiber layers. Nevertheless, there are no evident signs of single fiber pullout and debonding in the direction of the load. Instead, the fibers of 0° bundles are still together with the matrix surrounding them still intact, as seen in the higher magnification image of Fig. 6a. Therefore, it can be presumed that the whole fiber bundle was pulled out during loading. These observations are very similar to the ones made for the fracture surface of the as-processed composite. In contrast, samples tested after the fatigue loading of 80% and 90% show clear signs of single-filament fiber pullout. In the regions of pullout, the matrix around the fibers is damaged as there are only fragments of the matrix remaining (Fig. 6b).

4. Discussion

4.1. Damage development during fatigue loading

The studied PIP C/SiC composite shows very high fatigue limit at room temperature. To illustrate that, the relationship between applied fatigue stress level versus number of cycles to failure (S-N curve) are presented in Fig. 7. For comparison, literature values of C/SiC composites produced by chemical vapor infiltration (CVI) [10,23–25], as well as other SiC-based composites like C/C-SiC [17] and SiC/SiC [26] are also added to the S-N curve. It should be highlighted that the strength of SiC-based composites can greatly differ due to different processing parameters. The strength of the selected CVI C/SiC composites range from 211 to 420 MPa, while the C/C-SiC and SiC/SiC

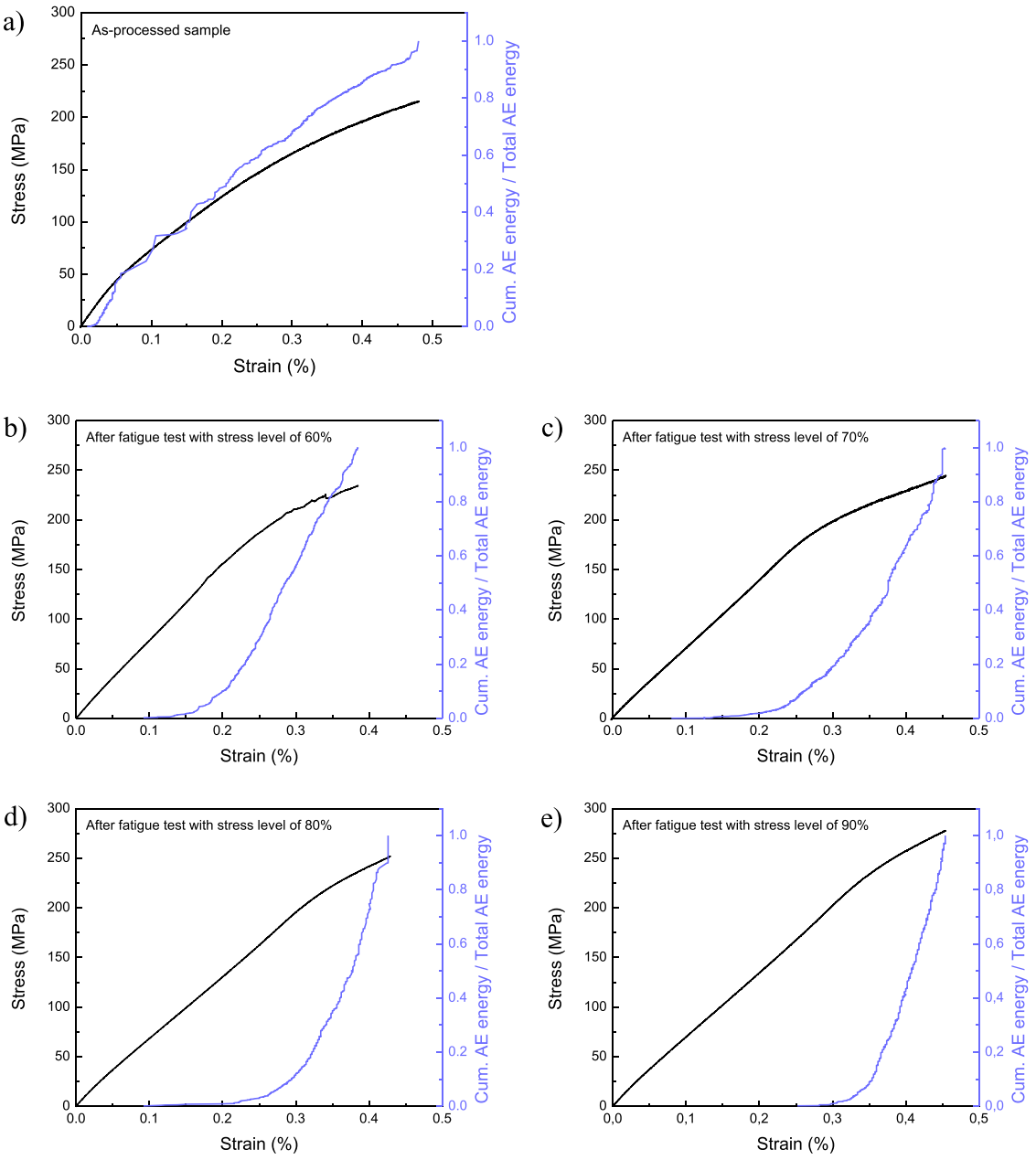

Fig. 4. Quasi-static tensile tests of (a) as-processed sample and after fatigue loading with 1,000,000 cycles and fatigue stress levels of (b) 60%, (c) 70%, (d) 80% and (e) 90%.

composites show tensile strength of 78 MPa and 209 MPa, respectively. Therefore, the comparison below is done regarding the stress level in relation to the respective composite tensile strength values. All specimens studied in this work survived the run-out of 1,000,000 cycles even with the stress level of 90% (195 MPa). As seen in Fig. 7, other SiC-based composites have fatigue limit ranging from 80% to 89% of their respective tensile strength when considering this run-out criteria. Fatigue life of CMCs depends mainly on the development and accumulation of damage, which in turn, depends on the composition of the composite, used fiber architecture, interface, processing and microstructure of the matrix, as well as testing parameters like frequency. In order to understand the high fatigue limit of this C/SiC composite, the damage development during the fatigue loading is analyzed below.

The damage analysis was performed by measuring the dynamic modulus, as well as the AE activity. As seen in Fig. 3, the dynamic modulus decreases while the AE hit count and energy increases as the loading progress for all fatigue tests. The decrease of dynamic modulus is commonly associated with the damage development during loading of CMCs since the generated damage changes the load-bearing volume of the sample [27]. The increase of AE energy corresponds very well with the decrease of dynamic modulus, in which both parameters drastically change during the cycles up to the maximum fatigue stress. However, the AE hit count shows a different tendency. In the literature, both AE hit count and AE energy have been used to describe the damage during the fatigue loading of CMCs [19,20]. Nevertheless, these two parameters have different meanings. While AE hit count can give information about time and frequency of damage, AE energy is also related to the associated damage mechanisms. As the C/SiC composites are loaded, different damage mechanisms can take place including matrix crack initiation and propagation, crack closing and re-opening, fiber-matrix debonding and pullout, fiber breakage, as well as friction and movement of the generated surfaces/defects. Each type of damage mechanism can have very distinct ranges of AE energy [28]. Therefore, the measured cumulative AE energy is a better representation of the damage developed

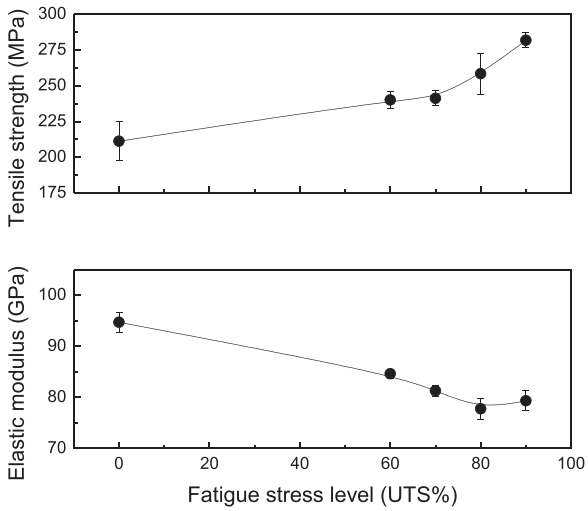

Fig. 5. Residual tensile strength and elastic modulus after fatigue loading with 1,000,000 cycles and different fatigue stress levels.

during fatigue loading of the studied composite.

According to Fig. 3, most of the fatigue damage occurs in the first cycles, especially during the first loading. As aforementioned, the proportional limit of the studied composite is of about 35 MPa. Above this stress, damage will take place, which results in the observed non-linear and permanent deformation. The elastic limit of PIP SiC-based composites is normally low due to processing-induced stresses and defects [29]. During processing, the formation of residual stresses and inherent defects such as micro-cracks and pores in the matrix can occur due to the shrinkage during pyrolysis, as well as the thermal expansion mismatch between fibers and matrix during cooling down to room temperature. Therefore, matrix crack initiation and propagation can happen at relatively low stresses, which can later lead to other damage mechanisms.

The measured AE energy can be used to estimate the relative amount of damage in the material. During the first loading cycle, AE signals with different features are measured. For the studied material, it is presumed that the low-energy signals, which start at lower stresses, are associated with matrix damage. Signals with higher energy, which can be associated to interface damage and later to fiber failure, start appearing as the applied stress increases towards the maximum fatigue stress. As seen in Fig. 3, dynamic modulus and total AE energy rapidly change within the first 20 cycles, meaning that most of the interface and fiber damage takes place early during fatigue loading. High-energy AE hits are measured until shortly after the applied stress reaches the maximum fatigue stress on cycle 50. It should also be highlighted that, with higher fatigue stress levels, a higher amount of AE energy is measured in the first cycles, meaning that more damage was generated. After reaching the maximum fatigue stress, the amount and intensity of new damage starts to decrease. The same can be observed when analyzing the hysteresis loops (Fig. 2b), in which their area first increases and then decreases. After about 1000 cycles, fewer new AE signals are measured, and the energy of the new AE signals stays rather constant and relatively low. These signals are probably related to further matrix crack propagation, crack closing and re-opening, as well as friction and movement of the new generated fracture surfaces and interfaces. This is an indication that the cracking of the material starts to stabilize at this early point in the fatigue test.

Although the AE monitoring was done only during the first 100,000 cycles, it is possible to see that damage continues to take place until the run-out is reached by observing the decrease of dynamic modulus. This

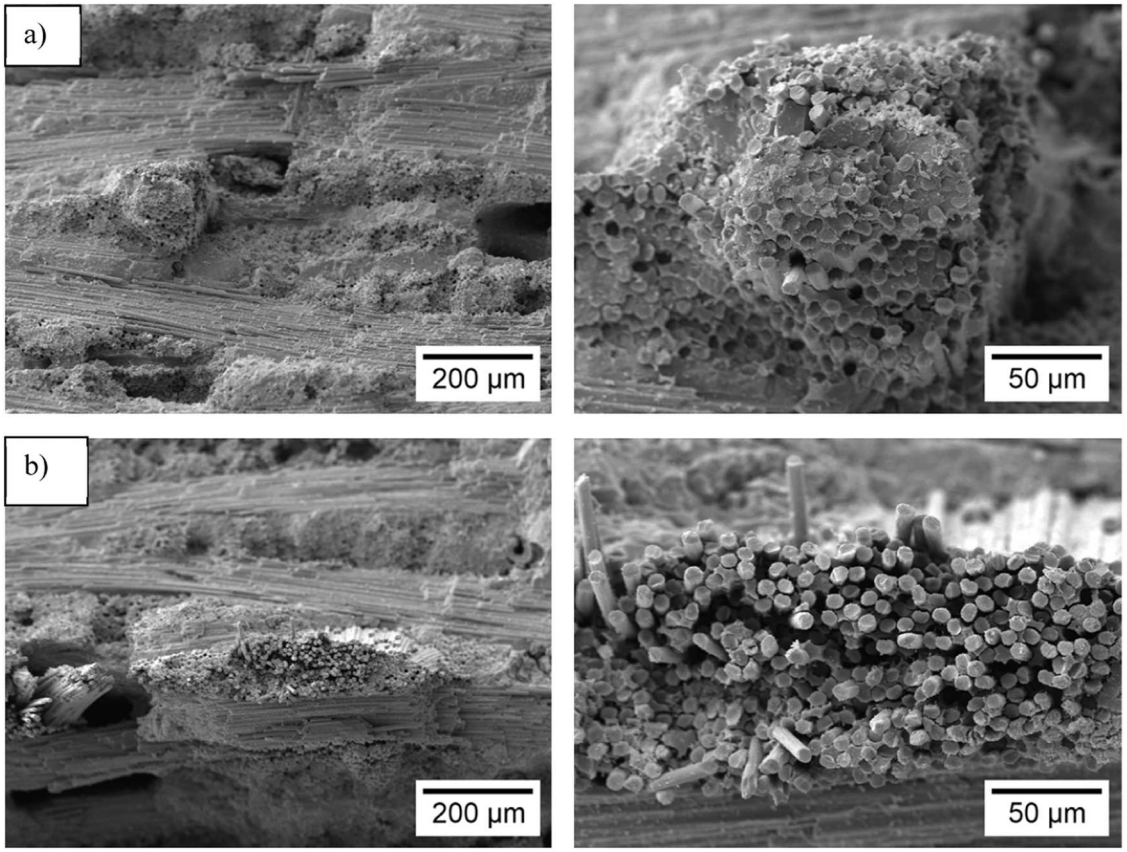

Fig. 6. SEM micrographs of the fracture morphology from quasi-static tensile test samples after fatigue loading with 1,000,000 cycles and fatigue stress levels of (a) 70% and (b) 90%.

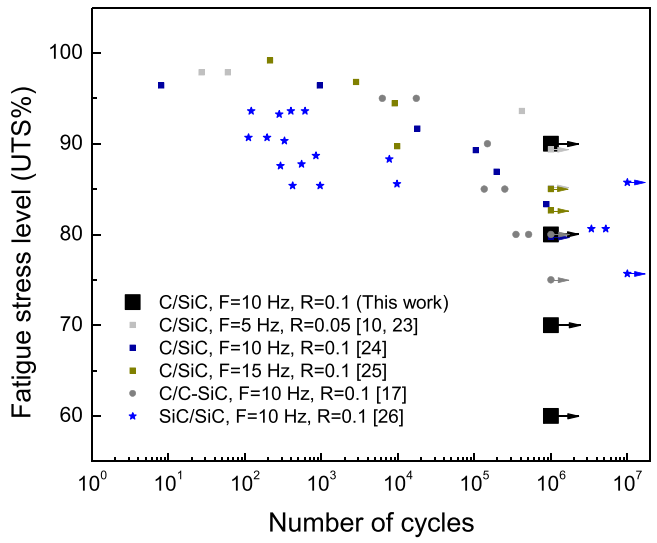

Fig. 7. S-N curve of tested PIP C/SiC composite and other SiC-based composites from the literature [10,17,23–26]. For reference, used test frequency (F) and stress ratio (R) are given. Arrows indicate that the samples survived the specified amount of run-out cycles.

is easier to perceive for samples tested with higher stress levels and is an indication that studied composite does not show a true fatigue limit. In other words, new damage can still take place if the material is loaded further. A true fatigue limit is hard to be determined for CMCs since microscopic damage can still occur [27]. Nevertheless, 1,000,000 cycles can be considered as a practical limit, considering the applications of such materials. Furthermore, it is expected that the microstructural changes, caused by fatigue loading after 1,000,000 cycles, would be much less severe than the damage promoted during the first cycles, as pointed out by the AE analysis. Hence, the studied C/SiC composite shows high fatigue strength. As previously mentioned, the mechanical behavior of SiC-based composites is influenced by the presence of process-induced stresses and defects. Still, due to the relatively low preparation temperature and repeated impregnation cycles, the possible micro-cracks caused by pyrolysis shrinkage and by the mismatch of thermal expansion coefficients are less prominent for this composite. Hence, the material shows relatively higher elastic limit in comparison to other C/SiC composites and the damage stabilizes earlier.

4.2. *Post-fatigue mechanical behavior*

The observed damage developed during the fatigue loadings also influences the post-fatigue mechanical properties of the composite. The mechanical behavior of the samples before and after the fatigue tests was measured with quasi-static tensile tests. In the as-processed state (before the fatigue loading), the composite shows predominantly a quasi-ductile behavior (Fig. 4a). As previously mentioned, this is related to the presence of residual stresses and defects in the matrix. As shown in Fig. 4a, AE activity is detected below the measured proportional limit. This is an indication that microscopic damage, possibly in the form of matrix cracking, can take place at lower stresses. However, it is presumed that this initial microscopic damage is considerably low. Therefore, no macroscopic changes in the stress-strain response are observed until reaching the proportional limit at 35 MPa. Similar observations have also been made for other types of CMCs in the literature [30–32]. Above the proportional limit, it can be presumed that the formation and growth of matrix cracks are more prominent. As the loading progresses, AE hits with higher energy (above 300 eu) are measured, which can be associated to interface failure and later to fiber breakage. At the maximum stress before failure, cascaded hits with much higher AE energy were measured, which is the result of multiple failure mechanisms taking place at the same time. In other words, multiple fiber and matrix breakage. For the fatigue-loaded samples, the linear-elastic portion of the stress-strain curves is much bigger. New damage, i.e., AE signals and non-linear deformation, is only observed above the previous maximum fatigue stress. After reaching the proportional limit however, the progression of damage is faster with higher fatigue stress levels.

As seen in Fig. 5, there is an overall decrease of the elastic modulus after the fatigue loadings until the fatigue stress level of 80%, after which the measured elastic modulus is constant. This decrease of elastic modulus is mainly related to the formation and growth of matrix cracks throughout the fatigue loadings. Hence, higher fatigue stress level will lead to higher amount of matrix damage until reaching a "saturated" state. It is interesting to see that the elastic modulus of the samples after the fatigue loading of 80% does not show significant statistical differences when compared to samples after the fatigue loading of 90%, suggesting that the matrix damage is saturated. This is the opposite of what was observed during the fatigue loadings when analyzing the dynamic modulus (Fig. 3c and d), which constantly decreases until the end of the fatigue test and reaches a lower value when the sample is loaded with the stress level of 90% in comparison to 80%. This is an indication that part of the fatigue damage is "healed" during the unloading of the composite. This effect can be due to matrix cracks that partially close, as well as matrix or interface defects that move back to their original position when the fatigue stress is released.

Contrary to the measured elastic modulus, the tensile strength of the composites increases with the fatigue stress level even though the fatigue loading promotes damage. The increase of tensile strength after fatigue loadings of SiC-based composites is normally associated with the reduction of the process-induced internal stresses [10,17]. The formation and propagation of matrix cracks during the fatigue loading dissipates mechanical energy, which can reduce the internal stress state of the as-processed composite. Thus, resulting in an increase of tensile strength (Fig. 5) and damage onset (Fig. 4). Furthermore, the fatigue damage can also weaken the fiber-matrix interface depending on the fatigue stress level. As commonly known, the strength of the fiber-matrix interface can influence the mechanical behavior of CMCs by facilitating crack deflection. Since the fracture patterns of samples fatigue loaded up to 70% (Fig. 6a) are similar to the as-processed samples, it can be assumed that there is no significant interface damage at this point. For the higher fatigue stress levels, more signs of fiber pullout were seen along the fracture surface (see Fig. 6b), indicating that the interface was weakened during the fatigue loading. It is suggested that at higher stresses, there will be more fiber debonding during the first fatigue cycles. Therefore, the tensile strength increase observed after the fatigue loadings of 80% and 90% is relatively much higher than after 60% and 70%. This interfacial damage may not influence the measured elastic modulus of the composite. Hence, samples after the fatigue loading of 80% and 90% show similar elastic modulus, but different tensile strength.

5. Conclusions

In the present study, the fatigue behavior of a PIP C/SiC composite was studied. For that, tensile fatigue tests with stress levels of 60–90% of the composite tensile strength were performed. The material showed very high fatigue limit considering that all samples survived the run-out of 1,000,000 cycles. In comparison, other SiC-based composites normally show fatigue limit below 90%. The development of fatigue damage during loading was analyzed by measuring the dynamic modulus and AE activity. The measured AE energy proved to be a good indication for the fatigue damage as it gives information not only on the frequency of damage, but also about its source. In this sense, it is suggested that matrix cracking, interface damage and fiber breakage occurs in the first cycles as the applied stress reaches the maximum fatigue stress. As the loading progress, new damage in the form of matrix crack opening and closing as well as interfacial friction gradually accumulates without

leading the failure of the composite. Therefore, the high fatigue strength was mainly associated with the high density of the matrix.

After the fatigue loadings, the mechanical behavior of the C/SiC composite under quasi-static tensile stress drastically changes. The composite starts to show a more linear-elastic behavior and new substantial damage only occurs after the maximum fatigue stress is reached. In this sense, the elastic modulus of the composites decreases until reaching a plateau at fatigue stress levels equal or above to 80%. This is an indication that part of the fatigue damage is recovered during the unloading. Although the fatigue damage decreases the elastic modulus of the studied composite, an increase of tensile strength was observed after the fatigue tests. This was related to the relief of process-induced stresses due to the fatigue damage. In addition, fracture analysis indicated that considerable interface damage takes place when the fatigue stress level is above 80%. As the weakening of the interface facilitates damage mechanisms like fiber debonding and pullout, the strength of the composite increases.

CRediT authorship contribution statement

Renato S. M. Almeida: Conceptualization, Methodology, Validation, Formal analysis, Investigation, Data curation, Writing - Original Draft, Visualization, **Si'an Chen**: Conceptualization, Methodology, Resources, Data curation, Writing - Review & Editing, Project administration, Funding acquisition, **Benjamin Besser**: Formal analysis, Writing - Review & Editing, Visualization, **Kamen Tushtev**: Validation, Data Curation, Writing - Review & Editing, **Yang Li**: Conceptualization, Methodology, Validation, Formal analysis, Data curation, Writing - Review & Editing, Supervision, Project administration, Funding acquisition, **Kurosch Rezwan**: Validation, Resources, Writing - Review & Editing, Supervision, All authors have read and agreed to the published version of the manuscript.

Declaration of Competing Interest

The authors declare that they have no known competing financial interests or personal relationships that could have appeared to influence the work reported in this paper.

Acknowledgments

The authors gratefully acknowledge the financial support from the National Natural Science Foundation of China (grant no. 52102122 and 52173306). In addition, the authors thank Jürgen Horvath and Sofía G. M. Anaya for the help with the mechanical tests.

References

[1] R. Naslain, Design, preparation and properties of non-oxide CMCs for application in engines and nuclear reactors: an overview, Compos. Sci. Technol. 64 (2) (2004) 155–170.
[2] W. Krenkel, F. Berndt, C/C–SiC composites for space applications and advanced friction systems, Mater. Sci. Eng. A 412 (1–2) (2005) 177–181.
[3] R. Naslain, F. Christin, SiC-matrix composite materials for advanced jet engines, MRS Bull. 28 (9) (2003) 654–658.
[4] N.P. Bansal, J. Lamon, Ceramic Matrix Composites: Materials, Modeling and Technology, John Wiley & Sons, 2014.
[5] A. Mühlratzer, H. Pfeiffer, CMC Body Flaps for the X-38 Experimental Space Vehicle, 26th Annual Conference on Composites, Advanced Ceramics, Materials, and Structures: A: Ceramic Engineering and Science Proceedings2002, pp. 331–338.
[6] H. Ohnabe, S. Masaki, M. Onozuka, K. Miyahara, T. Sasa, Potential application of ceramic matrix composites to aero-engine components, Compos. Part A Appl. Sci. Manuf. 30 (4) (1999) 489–496.
[7] L. Longbiao, Comparison of cyclic fatigue behavior between C/SiC and SiC/SiC ceramic-matrix composites at elevated temperatures using hysteresis dissipated energy, Compos. Struct. 150 (2016) 41–52.
[8] L. Longbiao, Cyclic loading/unloading hysteresis behavior of fiber-reinforced ceramic–matrix composites at room and elevated temperatures, Mater. Sci. Eng. A 648 (2015) 235–242.
[9] K.G. Dassios, D.G. Aggelis, E.Z. Kordatos, T.E. Matikas, Cyclic loading of a SiC-fiber reinforced ceramic matrix composite reveals damage mechanisms and thermal residual stress state, Compos. Part A Appl. Sci. Manuf. 44 (2013) 105–113.
[10] G. Fang, X. Gao, G. Yu, S. Zhang, J. Chen, Y. Song, Effect of the stress level on the fatigue strengthening behavior of 2D needled C/SiC CMCs at room temperature, Mater. Des. 89 (2016) 432–438.
[11] M.B. Ruggles-Wrenn, T.P. Jones, Tension–compression fatigue of a SiC/SiC ceramic matrix composite at 1200°C in air and in steam, Int. J. Fatigue 47 (2013) 154–160.
[12] Y. Li, P. Xiao, W. Zhou, H. Luo, Z. Li, Microstructure and properties of plain-weave carbon fabric reinforced ceramic composites containing Cu-Si alloy, Compos. Part B Eng. 145 (2018) 129–135.
[13] Y. Li, P. Xiao, Z. Li, W. Zhou, T. Liensdorf, W. Freudenberg, N. Langhof, W. Krenkel, Tensile fatigue behavior of plain-weave reinforced Cf/C–SiC composites, Ceram. Int. 42 (6) (2016) 6850–6857.
[14] C. Liu, D. Shi, X. Jing, R. Luo, L. Wang, X. Yang, Multiscale investigation on fatigue properties and damage of a 3D braided SiC/SiC + PyC/SiC composites in the full stress range at 1300 °C, J. Eur. Ceram. Soc. 42 (4) (2022) 1208–1218.
[15] Y. Xue, J. Hu, H. Zhou, L. Li, Q. Shan, Y. Kan, L. Gao, S. Dong, Damage development of a woven SiCf/SiC composite during multi-step fatigue tests at room temperature, Ceram. Int. 46 (14) (2020) 22116–22126.
[16] G. Hou, D.-G. Shang, L.-X. Zuo, L.-F. Qu, Y.-E. Guo, M. Xia, S.-D. Wu, X. Yin, Fatigue damage identification of SiC coated needled C/SiC composite by acoustic emission, Ceram. Int. 47 (11) (2021) 15129–15138.
[17] Y. Li, P. Xiao, H. Luo, R.S.M. Almeida, Z. Li, W. Zhou, A. Brückner, F. Reichert, N. Langhof, W. Krenkel, Fatigue behavior and residual strength evolution of 2.5D C/C-SiC composites, J. Eur. Ceram. Soc. 36 (16) (2016) 3977–3985.
[18] G.N. Morscher, A.L. Gyekenyesi, The velocity and attenuation of acoustic emission waves in SiC/SiC composites loaded in tension, Compos. Sci. Technol. 62 (9) (2002) 1171–1180.
[19] G.N. Morscher, Stress-dependent matrix cracking in 2D woven SiC-fiber reinforced melt-infiltrated SiC matrix composites, Compos. Sci. Technol. 64 (9) (2004) 1311–1319.
[20] R.S.M. Almeida, Y. Li, B. Besser, P. Xiao, W. Zhou, A. Brückner, N. Langhof, K. Tushtev, W. Krenkel, K. Rezwan, Damage analysis of 2.5D C/C-SiC composites subjected to fatigue loadings, J. Eur. Ceram. Soc. 39 (7) (2019) 2244–2250.
[21] S. Momon, M. Moevus, N. Godin, M. R'Mili, P. Reynaud, G. Fantozzi, G. Fayolle, Acoustic emission and lifetime prediction during static fatigue tests on ceramic-matrix-composite at high temperature under air, Compos. Part A Appl. Sci. Manuf. 41 (7) (2010) 913–918.
[22] K. Jian, Z.-H. Chen, Q.-S. Ma, W.-W. Zheng, Effects of pyrolysis processes on the microstructures and mechanical properties of Cf/SiC composites using polycarbosilane, Mater. Sci. Eng. A 390 (1) (2005) 154–158.
[23] G. Fang, X. Gao, S. Zhang, J. Xue, Y. Song, F. Wang, A residual strength model for the fatigue strengthening behavior of 2D needled CMCs, Int. J. Fatigue 80 (2015) 298–305.
[24] S.F. Shuler, J.W. Holmes, X. Wu, D. Roach, Influence of loading frequency on the room-temperature fatigue of a carbon-fiber/SiC-matrix composite, J. Am. Ceram. Soc. 76 (9) (1993) 2327–2336.
[25] C. Zhang, X. Wang, Y. Liu, B. Wang, D. Han, S. Qiao, Y. Guo, Tensile fatigue of a 2.5D-C/SiC composite at room temperature and 900°C, Mater. Des. 49 (2013) 814–819.
[26] S. Zhu, M. Mizuno, Y. Kagawa, Y. Mutoh, Monotonic tension, fatigue and creep behavior of SiC-fiber-reinforced SiC-matrix composites: a review, Compos. Sci. Technol. 59 (6) (1999) 833–851.
[27] B.F. Sørensen, J.W. Holmes, E.L. Vanswijgenhoven, Does a true fatigue limit exist for continuous fiber-reinforced ceramic matrix composites? J. Am. Ceram. Soc. 85 (2) (2002) 359–365.
[28] C. Xie, X. Gao, H. Zhang, Y. Song, Multiscale acoustic emission of C/SiC mini-composites and damage identification using pattern recognition, Sci. Eng. Compos. Mater. 27 (1) (2020) 148–162.
[29] H. Mei, Measurement and calculation of thermal residual stress in fiber reinforced ceramic matrix composites, Compos. Sci. Technol. 68 (15) (2008) 3285–3292.
[30] G.N. Morscher, H.M. Yun, J.A. DiCarlo, In-plane cracking behavior and ultimate strength for 2D Woven and braided melt-infiltrated SiC/SiC composites tensile loaded in off-axis fiber directions, J. Am. Ceram. Soc. 90 (10) (2007) 3185–3193.
[31] M. Surgeon, E. Vanswijgenhoven, M. Wevers, O. Van Der Biest, Acoustic emission during tensile testing of SiC-fibre-reinforced BMAS glass-ceramic composites, Compos. Part A Appl. Sci. Manuf. 28 (5) (1997) 473–480.
[32] R.Y. Kim, N.J. Pagano, Crack initiation in unidirectional brittle-matrix composites, J. Am. Ceram. Soc. 74 (5) (1991) 1082–1090.